Check for updates

Journal of Biomedical Materials Research Part A

WILEY

Society For Biomaterials

RESEARCH ARTICLE

A Novel Radially Graded Hydroxyapatite-Based Composite for Bioactive Implant Interfaces

Zeliha Coskun Tas[1] | Talip Celik[1] | Ibrahim Mutlu[1] | Ridvan Yamanoglu[2] | Lorna Anguilano[3]

[1]Faculty of Technology, Biomedical Engineering Department, Kocaeli University, Kocaeli, Turkey | [2]Faculty of Engineering, Metallurgical and Materials Engineering Department, Kocaeli University, Kocaeli, Turkey | [3]Experimental Techniques Centre, Brunel University London, London, UK

Correspondence: Zeliha Coskun Tas (zeliha.coskun@kocaeli.edu.tr)

Received: 6 July 2025 | **Revised:** 29 September 2025 | **Accepted:** 9 October 2025

Funding: This work was supported by Scientific Research Project Unit of Kocaeli University, FDK-2023-3445, FHD-2024-3657; the Scientific and Technological Research Council of Türkiye (TUBITAK), 2211-C 2023/1, 2214-A 2023/2.

Keywords: bioactive interface | FGM | hydroxyapatite | Ti-5Mo alloy

ABSTRACT

The combination of superior mechanical properties, corrosion resistance, and biological characteristics makes Ti-6Al-4V a widely used biomaterial. However, its clinical application as an orthopedic implant is limited by its hardness and weak osseointegration capacity. This study focuses on the development of a functionally graded biomaterial that has increased bioactivity and decreased mechanical mismatch with living tissue. In this scope, a novel radially functionally graded Ti-5Mo/hydroxyapatite (HA) biocomposite was successfully fabricated via pressure-assisted sintering using a specially designed mold that enabled directional HA enrichment toward the outer surface. This architectural design addresses the persistent challenge of combining mechanical reliability with biological functionality in load-bearing implants. Comprehensive characterization was performed, including x-ray diffraction (XRD), Rietveld refinement, optical and scanning electron microscopy (SEM/EDX), atomic force microscopy (AFM), contact angle measurements, and in vitro cytotoxicity assays using L929 fibroblast cells. Mechanical behavior was assessed through Brazilian splitting, three-point bending, microhardness, and tribological testing under both dry and corrosive conditions. The biocomposite exhibited a dual-phase $\alpha+\beta$ titanium matrix and HA-derived oxides in the surface layers, with a graded increase in porosity and hardness from the core to the periphery. Mechanical tests revealed a bending modulus of 22.4 GPa, close to that of cortical bone, while the surface showed enhanced roughness, hydrophilicity (contact angle 35.3°), and corrosion resistance. In vitro results confirmed the material's biocompatibility and superior cell viability in HA-rich regions. These findings demonstrate that the developed Ti-5Mo/HA FGM offers a structurally and biologically optimized solution for orthopedic and dental implant applications.

1 | Introduction

Titanium (Ti) and its alloys, particularly Ti-6Al-4V, have been extensively used in orthopedic implants due to their superior mechanical strength, corrosion resistance, and biocompatibility [1, 2]. Despite these advantages, conventional Ti-based materials exhibit a significant mismatch in elastic modulus compared to natural bone, leading to the well-known stress shielding effect [3, 4]. This phenomenon impairs normal bone remodeling, reduces osseointegration, and ultimately contributes to implant loosening and failure, often necessitating costly and complex revision surgeries [5]. Addressing this critical challenge requires the development of biomaterials that can simultaneously minimize mechanical mismatch and enhance osseointegration through advanced structural and compositional strategies [6, 7]. One promising approach involves the development of hybrid and functionally graded materials (FGMs), which enable a gradual variation in composition and

© 2025 Wiley Periodicals LLC.

structure within a single component [5, 6]. FGMs are engineered to mimic the gradual changes found in natural biological systems, thus offering superior mechanical and biological compatibility [7]. In the field of orthopedics, metallic–ceramic FGMs that combine the mechanical strength of metals with the bioactivity of ceramics have emerged as a promising class of materials [6, 8, 9]. Hydroxyapatite (HA), a calcium phosphate-based bioceramic, closely resembles the mineral phase of bone and is widely employed in hard tissue engineering due to its excellent osteoconductivity and bioactivity [8, 10]. However, HA is intrinsically brittle and lacks the mechanical resilience required for load-bearing applications [11]. Therefore, HA is often incorporated into Ti matrices to balance bioactivity and mechanical strength [12]. Among Ti-based alloys, β-phase Ti alloys such as Ti-Mo have gained considerable attention due to their low elastic modulus, favorable mechanical properties, and excellent biocompatibility [13, 14]. Molybdenum (Mo), a non-toxic β-stabilizer, enhances the corrosion resistance and strength of Ti alloys while reducing their stiffness [15]. Ti-5Mo, in particular, exhibits a single β-phase structure, making it a suitable candidate for biomedical applications [16, 17].

Previous studies have mostly focused on longitudinally graded or bilayer composite structures, with limited attention given to radially graded configurations [6, 10, 11]. However, radially graded implants may offer enhanced stress distribution, improved interfacial bonding, and better mimicry of natural bone architecture, especially in cylindrical bone-replacing implants [13, 14]. Despite their potential advantages, studies on the development and characterization of radially graded metallic–ceramic composites remain scarce [5, 10, 14].

In this context, the present study aims to design and fabricate a novel radially graded Ti-5Mo/HA biocomposite using a pressure-assisted sintering technique with a specially designed mold architecture. The radial gradation is intended to produce a metallic core for mechanical support and an HA-rich outer region for bioactivity. The microstructural, mechanical, corrosion, and cytocompatibility properties of the developed composite are comprehensively investigated to evaluate its potential as a load-bearing orthopedic implant material.

2 | Materials and Methods

2.1 | Material Preparation

Commercial Ti-6Al-4V powder (ASTM Grade 5, average particle size: 44 μm), Mo powder (99.95% purity, particle size: 1–10 μm), and HA powder (99.5% purity, particle size: 40–50 μm) were used to fabricate the radially graded Ti-5Mo/HA composites. The Ti-6Al-4V powder was obtained from Alpomet Ltd., whereas the Mo and HA powders were supplied by Nanografi Nano Technology Inc.

To achieve the desired functional gradation, three distinct powder compositions were prepared to form layered cylindrical samples (5 mm in height and 20 mm in diameter), as summarized in Table 1. Mo, a β-phase stabilizer, was incorporated at a constant 5 wt.% in all layers, based on prior studies [15]. This concentration was selected to promote β-phase formation while maintaining mechanical integrity. Higher Mo content can result in the formation of brittle undissolved phases, whereas lower concentrations may be insufficient for effective stabilization. The innermost core layer was designed to maximize mechanical strength and consisted of 95 wt.% Ti-6Al-4V and 5 wt.% Mo. To enhance bioactivity in the outer regions, the HA content was progressively increased: 5 wt.% in the middle layer (TiMo5HA) and 10 wt.% in the outermost layer (TiMo10HA).

TABLE 1 | Composition of each layer in the radially graded Ti-5Mo/HA composite (wt.%).

Layer	Ti-6Al-4V	Mo	HA
Inner layer (TiMo)	95	5	—
Middle layer (TiMo5HA)	90	5	5
Outer layer (TiMo10HA)	85	5	10

2.2 | Powder Mixing and Consolidation

The powders designated for each layer were mechanically mixed for 45 min using a planetary ball mill equipped with zirconia jars and 5 mm diameter zirconia balls. Mixing was performed under vacuum conditions (10^{-2} mbar) at a rotation speed of 300 rpm to minimize the risk of contamination and oxidation. The homogenized powders were then sequentially introduced into a custom-designed mold that enables precise radial gradation. This specialized mold design, which allows for controlled layer deposition, is currently the subject of a pending patent application. A schematic illustration of the radial gradation process and the mold configuration is presented in Figure 1. To prevent powder adhesion during compaction, graphite paper was inserted between the powder layers and the inner walls of the graphite mold.

2.3 | Sintering Process

The loaded mold was transferred to a vacuum hot press furnace (DIEX, Korea) for sintering. The process was conducted under high vacuum conditions (10^{-4} mbar) to minimize oxidation. Sintering was carried out at 950°C for 45 min under a constant uniaxial pressure of 45 MPa. After sintering, the samples were allowed to cool to room temperature inside the furnace under vacuum, thereby preventing thermal shock and further oxidation.

2.4 | Metallographic Preparation

The sintered samples were sequentially ground using silicon carbide abrasive papers with grit sizes ranging from 320 to 2000. Final polishing was carried out with diamond suspensions of 6, 3, and 1 μm to achieve a smooth surface suitable for subsequent microstructural and mechanical characterization.

2.5 | Phase and Microstructural Characterization

The phase compositions of the starting powders and sintered Ti-5Mo/HA functionally graded samples were analyzed using

15524965, 2025, 11, Downloaded from https://onlinelibrary.wiley.com/doi/10.1002/jbm.a.38007 by ibrahim mutlu - Kocaeli Üniversitesi , Wiley Online Library on [03/11/2025]. See the Terms and Conditions (https://onlinelibrary.wiley.com/terms-and-conditions) on Wiley Online Library for rules of use; OA articles are governed by the applicable Creative Commons License

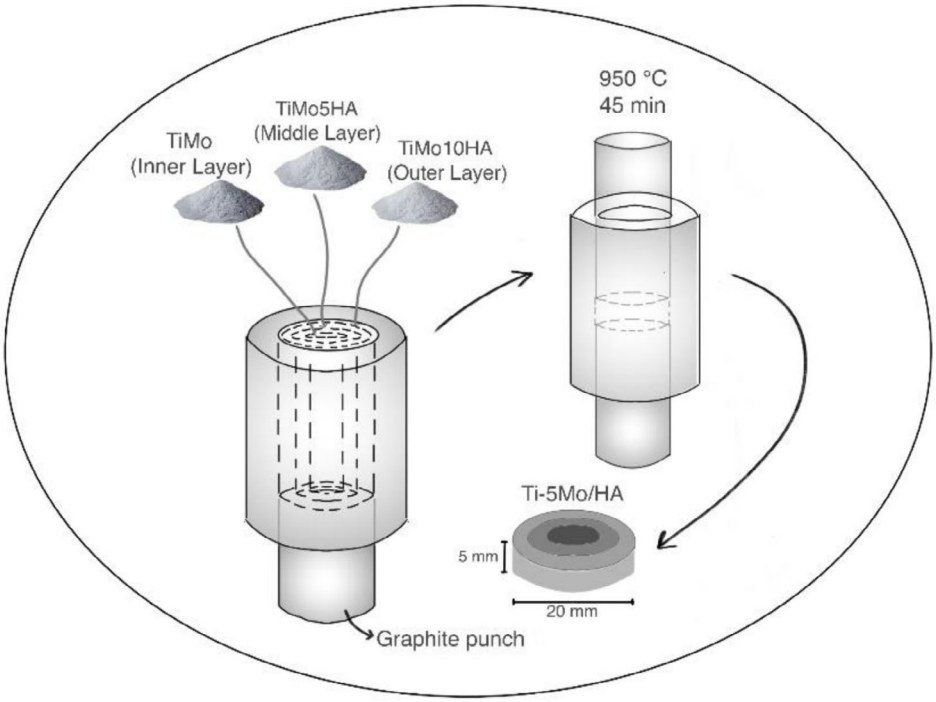


FIGURE 1 | Schematic illustration of the radial gradation design and mold configuration used for the Ti-5Mo/HA composite production.

TABLE 2 | Phase information and ICSD references for quantitative XRD analysis.

Phase	ICSD code	Phase	ICSD code
Mo_2Ti	253,843	TiV	150,817
TiO	20,041	HA	26,204
Ti	44,390	Ti6Al4V	58,190
Ti_6O	20,042	Al_4Ti	604,461
TiPO	83,937		

x-ray diffraction (XRD, Bruker D8 Advance, Germany) with Cu-K radiation ($\lambda = 0.1541$ nm, 40 kV). Diffraction patterns were collected over a 2 range of 10° to 100°, with a step size of 0.02°. Initial microstructural observations were conducted using optical microscopy (OM, Zeiss Axioscope 2 Mat), followed by detailed surface and compositional analyses using a scanning electron microscope (SEM, Jeol IT200 LV) equipped with energy-dispersive X-ray spectroscopy (EDX, Oxford Instruments, UK).

Quantitative phase analysis was performed via Rietveld refinement using TOPAS software, which applies a general non-linear least-squares fitting algorithm to the XRD data. Based on atomic percentage results obtained from SEM–EDX, crystal structure files corresponding to Mo_2Ti, TiO, Ti, Ti_6O, TiPO, TiV, HA, Ti-6Al-4V, and Al_4Ti phases were imported into TOPAS for refinement. All identified phases, along with their corresponding ICSD (Inorganic Crystal Structure Database) codes, are listed in Table 2. Microstructural observations were carried out on radial cross-sections of the Ti-5Mo/HA samples to evaluate compositional and structural gradients.

2.6 | Surface Topography Characterization

Surface topography plays a pivotal role in the integration of biomaterials with living tissues by directly affecting cellular responses and tissue attachment. In this study, the three-dimensional (3D) surface topography and contact potential difference of the Ti-5Mo/HA functionally graded samples were analyzed using atomic force microscopy (AFM, Dimension 3100, Santa Barbara, USA). Measurements were conducted in tapping mode at a scan frequency of 3 Hz, utilizing standard Si_3N_4 tips. Each individual layer of the Ti-5Mo/HA specimen was separately examined to assess surface roughness characteristics. 3D topographical images were obtained over a scan area of $100\,\mu m \times 100\,\mu m$, and corresponding quantitative surface roughness parameters were recorded.

2.7 | Mechanical Characterization

The mechanical properties of the Ti-5Mo/HA functionally graded samples were evaluated through Brazilian splitting tensile tests, three-point bending tests, Vickers hardness measurements, and wear tests conducted under both dry and corrosive conditions.

The Brazilian splitting tensile test was carried out in accordance with ASTM C496/C496M-04, which is specifically designed for cylindrical samples where conventional tensile testing is impractical due to geometric limitations [18–20]. The tests were performed using a hydraulic universal testing machine equipped with a 1200 kN load cell, at a constant loading rate of 1 mm/min. Curved loading pads were placed on the top and bottom of the specimens to ensure proper alignment and load distribution during testing. Load and displacement data were recorded in real time using a National Instruments data acquisition system

15524965, 2025, 11, Downloaded from https://onlinelibrary.wiley.com/doi/10.1002/jbm.a.38007 by ibrahim mutlu - Kocaeli Üniversitesi , Wiley Online Library on [03/11/2025]. See the Terms and Conditions (https://onlinelibrary.wiley.com/terms-and-conditions) on Wiley Online Library for rules of use; OA articles are governed by the applicable Creative Commons License

connected to a PC. The applied compressive load (P) generated a tensile stress distribution along the sample height (H) and split length (L). The splitting tensile strength (σ) was calculated using Equation (1).

$$\sigma = \frac{2P}{\pi LH} \quad (1)$$

For the three-point bending tests, the samples were sectioned using a precision cutter (Metkon Microcut 150) to dimensions of $2 \times 3.5 \times 20$ mm, ensuring the integrity of the layered structure. The tests were carried out using a universal testing machine (INSTRON Universal 5985) in accordance with ASTM E290. The bending load was applied at the midpoint of each sample, perpendicular to its longitudinal axis, at a displacement rate of 2 mm/min until fracture. Stress–strain curves were continuously recorded during the tests.

Vickers hardness measurements were performed following ASTM E384-11 to evaluate the influence of the graded architecture on hardness distribution. A load of 0.2 kgf was applied with a dwell time of 10 s. Measurements were initiated from the central axis of the sample, and a total of 56 points were recorded at 0.15 mm intervals.

The wear resistance of the Ti-5Mo/HA functionally graded samples was assessed using a linear reciprocating ball-on-disk tribometer (UTS Tribometer T10) according to ASTM G133-05. Tests were conducted at room temperature under both dry and corrosive sliding conditions, applying a normal load of 20 N. Corrosive wear tests were carried out using artificial body fluid to simulate physiological environments. The total sliding distance was set to 100 m with a stroke length of 15 mm and a sliding frequency of 3 Hz. Steel balls were used as the counterface material. Mass loss was determined using an electronic balance with an accuracy of 0.01 mg to quantify material removal after testing. The specific wear rate (W) was calculated using Equation (2), where ΔV is the volumetric material loss (mm^3), P is the applied normal load (N), and S is the sliding distance (m) [21].

$$W = \frac{\Delta V}{P \cdot S} \quad (2)$$

2.8 | Wettability Analysis

Surface modifications of titanium implants have been extensively studied to enhance surface wettability and hydrophilicity, both of which are critical for protein adsorption and cellular interactions [22, 23]. Numerous studies have emphasized the significance of surface wettability in promoting favorable biological responses [24, 25]. In this study, wettability was assessed by measuring the static contact angle, also referred to as the equilibrium contact angle (θ_E), which reflects surface energy and hydrophilic behavior. However, contact angle values may fluctuate over time due to surface contamination, roughness, droplet spreading, and evaporation. To ensure a precise and comprehensive evaluation, advancing contact angle (ACA), receding contact angle (RCA), and contact angle hysteresis (CAH) were measured during droplet spreading and withdrawal. Prior to testing, the Ti-5Mo/HA samples were sequentially cleaned with distilled water, acetone, and ethanol, followed by drying under a nitrogen (N_2) stream. A droplet ($8 \pm 1\,\mu L$) of deionized water was carefully placed on the sample surface, and the ACA was measured after 10 s. Approximately one-third of the droplet volume was then withdrawn with a syringe, and the RCA was recorded. Contact angle measurements were performed using a contact angle analyzer (DMe-211 Plus, Kyowa Interface Science, Japan) equipped with a high-speed camera and backlight illumination. Data were analyzed using FTA32 software, and all measurements were conducted under ambient laboratory conditions with deionized water.

2.9 | Cytotoxicity Evaluation

The cytotoxicity of the Ti-5Mo/HA functionally graded samples was evaluated using L929 mouse fibroblast cells. Prior to testing, the Ti-5Mo/HA was divided into three equal segments (called Region 1, 2, and 3) using a precision cutter (Metkon Microcut 150) to dimensions of $3 \times 3 \times 3$ mm. Regions 1, 2, and 3 were cleaned with ethanol and sterilized under ultraviolet (UV) light for 120 min to eliminate potential contaminants. L929 mouse fibroblast cells were seeded into 96-well plates at a density of 3×10^5 cells per well and cultured in Low Glucose Dulbecco's Modified Eagle Medium (L-DMEM) growth medium supplemented with 1% Glutamax, 10% fetal bovine serum, and 1% penicillin/streptomycin at 37°C and 5% CO_2 for 24 h. Following incubation, cell viability and proliferation were assessed using the WST-1 Assay Kit (Roche Applied Science), in accordance with the manufacturer's instructions. The culture medium without material exposure was used as a negative control to establish baseline cell viability. All experiments were conducted in triplicate to ensure statistical accuracy, and the results were reported as the percentage of viable cells relative to the control group.

2.10 | Statistical Analysis

All experimental procedures were performed in replicates to ensure the reliability and reproducibility of the data. Mechanical tests were conducted in triplicate ($n = 3$), SEM–EDX analyses were performed at five different locations ($n = 5$), contact angle measurements were repeated six times ($n = 6$), and surface roughness assessments using AFM were carried out in triplicate ($n = 3$). Similarly, cytotoxicity assays were conducted in triplicate ($n = 3$) to evaluate cell viability. Statistical analyses were performed using one-way analysis of variance (ANOVA) and Student's t-test. Prior to hypothesis testing, data normality was assessed using the Shapiro–Wilk test. A p value less than 0.05 ($p < 0.05$) was considered statistically significant.

3 | Results

3.1 | Phase Analysis and Microstructural Characterization

Phase characterization is essential for understanding the correlation between microstructural evolution and the mechanical and biological performance of Ti-5Mo/HA FGMs. To this end, XRD analysis was conducted to identify phase constituents,

15524965, 2025, 11, Downloaded from https://onlinelibrary.wiley.com/doi/10.1002/jbm.a.38007 by ibrahim mutlu - Kocaeli Üniversitesi , Wiley Online Library on [03/11/2025]. See the Terms and Conditions (https://onlinelibrary.wiley.com/terms-and-conditions) on Wiley Online Library for rules of use; OA articles are governed by the applicable Creative Commons License

assess the effectiveness of β-phase stabilization via Mo addition, and verify the presence of HA in the graded structure. Figure 2 shows the XRD patterns of the Ti-5Mo/HA FGM. A distinct (011) reflection of the β-phase is observed at $2\theta = 40.4°$, confirming successful β-phase stabilization—especially within the core region.

Upon cooling, partial decomposition of the β-phase leads to the formation of α and martensitic α″ phases [26]. This transformation is most prominent in the inner layer, where β-phase intensity declines while α and α″ peaks dominate. The middle and outer layer powders retain a moderate amount of β-phase and display prominent HA peaks, verifying surface enrichment. Quantitative phase analysis using Rietveld refinement (TOPAS software) supports these findings (Figure 3). Major phases include TiO (33.91%), Ti_6O (24.09%), and TiPO (26.60%), all of which enhance surface reactivity and bioactivity. Minor phases detected include Mo_2Ti (2.59%), TiV (4.17%), Ti-6Al-4V (3.43%), and Al_4Ti (1.72%). Although HA was detected at only 0.01%, this is consistent with its surface localization, while XRD sampling focuses on the bulk. The calculated β-phase content (17.3%) significantly exceeds that of conventional Ti-6Al-4V alloys (~7.4%) [27], suggesting enhanced phase stability. Remaining constituents included 32.1% martensitic α″ and 50.5% α-phase, offering a balanced distribution for mechanical performance and biological compatibility.

Importantly, Mo-induced β-phase stabilization reduces the elastic modulus, better aligning the material's stiffness with that of natural bone. Refinement quality indicators confirm the robustness of the analysis, with GOF = 1.47, $R_exp = 10.15$, $R_wp = 14.97$, and $R_p = 11.24$ (Table 3), indicating excellent agreement between experimental and calculated patterns.

Figure 4a–c present optical microscopy images of the three layers. An equiaxed grain morphology is observed, with decreasing density from the core to the outer layer. The outer region exhibits porosity associated with HA inclusion. Figure 4d–f display SEM images, and corresponding EDX data are summarized in Table 4. Points 1–2 (Ti-rich regions) contain Ti, Al, and V, corresponding to the metallic matrix. Points 3–4 (Mo-rich) demonstrate increasing Mo content toward grain boundaries. Point 5 reveals Mo segregation zones, suggesting local phase concentration. EDX mapping confirms co-localization of Ti, Al, and V in matrix regions, while Mo preferentially aligns along grain boundaries (Figures S1–S3). Interlayer transition zones are visualized in Figures S4 and S5 via OM and SEM. Surface topography images from AFM

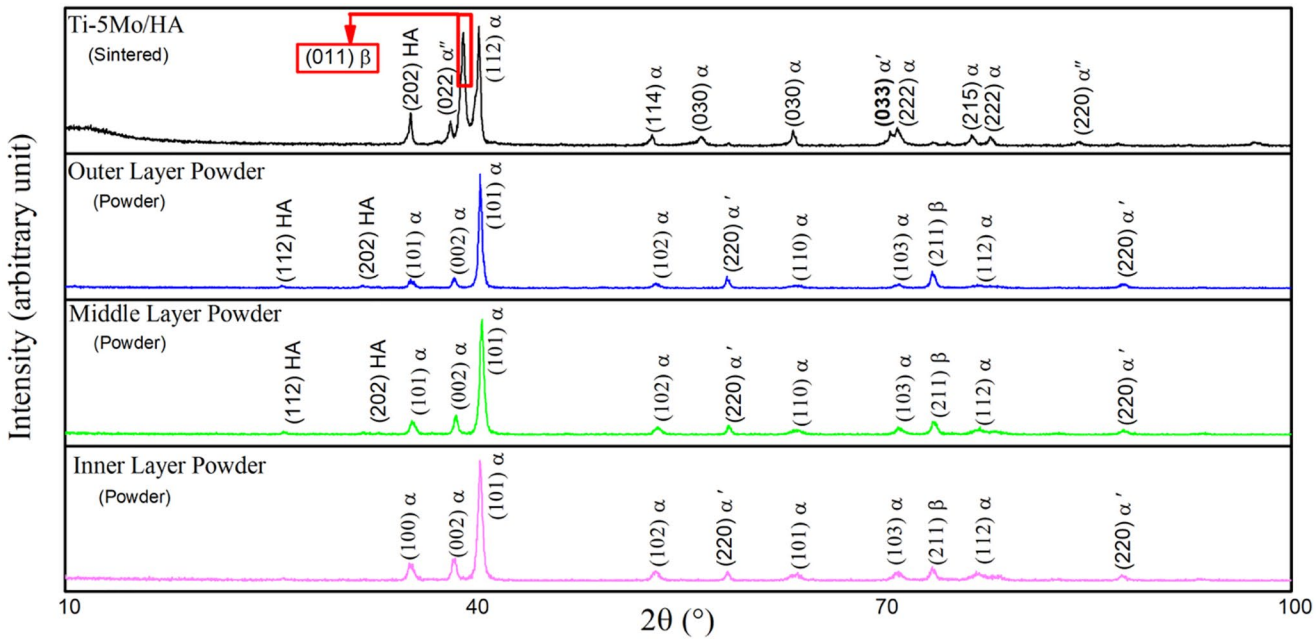


FIGURE 2 | XRD patterns of the bulk and layered powders of the Ti-5Mo/HA FGM.

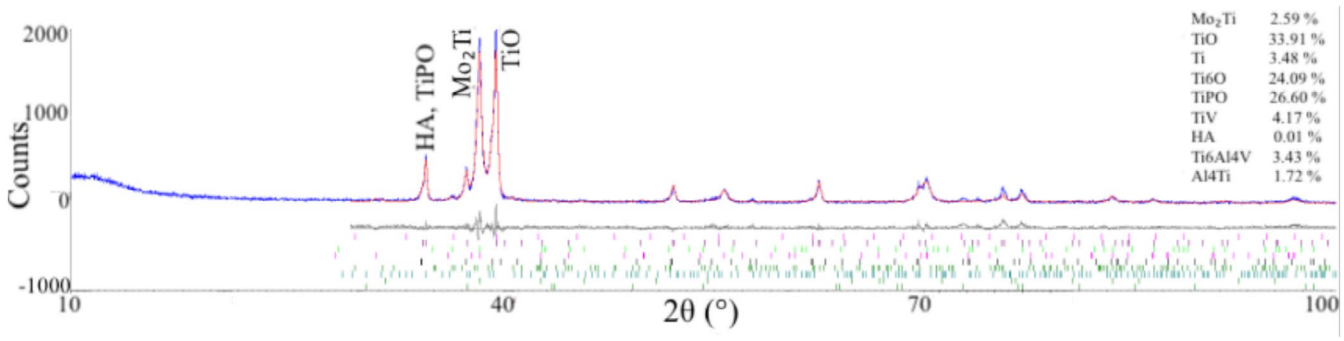


FIGURE 3 | Rietveld refinement results obtained using TOPAS software.

15524965, 2025, 11, Downloaded from https://onlinelibrary.wiley.com/doi/10.1002/jbm.a.38007 by ibrahim mutlu - Kocaeli Üniversitesi , Wiley Online Library on [03/11/2025]. See the Terms and Conditions (https://onlinelibrary.wiley.com/terms-and-conditions) on Wiley Online Library for rules of use; OA articles are governed by the applicable Creative Commons License

are shown in Figure 4g–i, with quantitative roughness metrics listed in Table 5. The root mean square roughness (Rq) increased from 145.2 ± 23.4 nm (inner layer) to 272.9 ± 96.9 nm (outer layer), while Ra values rose from 103 ± 19 nm to 148 ± 41 nm. This gradient correlates with increasing HA content. Notably, skewness (K) shifted from 0.391 (inner) to −3.91 (outer), indicating deeper valleys that enhance mechanical interlocking and cell anchorage [28]. These roughened, gradient surfaces are known to promote osseointegration and improve bone–implant interaction [29]. Overall, the combination of Mo-stabilized β-phase in the core and HA-enriched, roughened surfaces toward the exterior suggests the Ti-5Mo/HA FGM is well suited for biomedical applications requiring both mechanical durability and enhanced bioactivity.

TABLE 3 | TOPAS test results.

Material	GOF	R_{exp}	R_{wp}	R_p
Ti-5Mo/HA FGM	1.47	10.15	14.97	11.24

Abbreviations: GOF = goodness of fitting, R_{exp} = rietveld expected value, R_p = rietveld pattern, R_{wp} = rietveld weighted pattern.

4 | Mechanical Characterization

Mechanical characterization is essential to evaluate the structural integrity and functional performance of biomaterials intended for load-bearing implant applications. In this context, the Ti-5Mo/HA FGM developed in this study was subjected to comprehensive mechanical evaluations, including tensile, bending,

TABLE 4 | EDX analysis results for points 1–5 marked in Figure 3d–f of Ti-5Mo/HA SEM images.

	[wt.%]						
Point No.	**Ti**	**Al**	**V**	**Mo**	**O**	**P**	**Ca**
Point 1	86.6	6.1	3.4	3.8	—	—	—
Point 2	79.4	5.8	7.4	7.3	—	—	—
Point 3	73.9	5.5	4.0	16.6	—	—	—
Point 4	6.1	—	—	71.3	19.0	1.6	1.0
Point 5	7.0	—	0.5	88.5	4.0	—	—

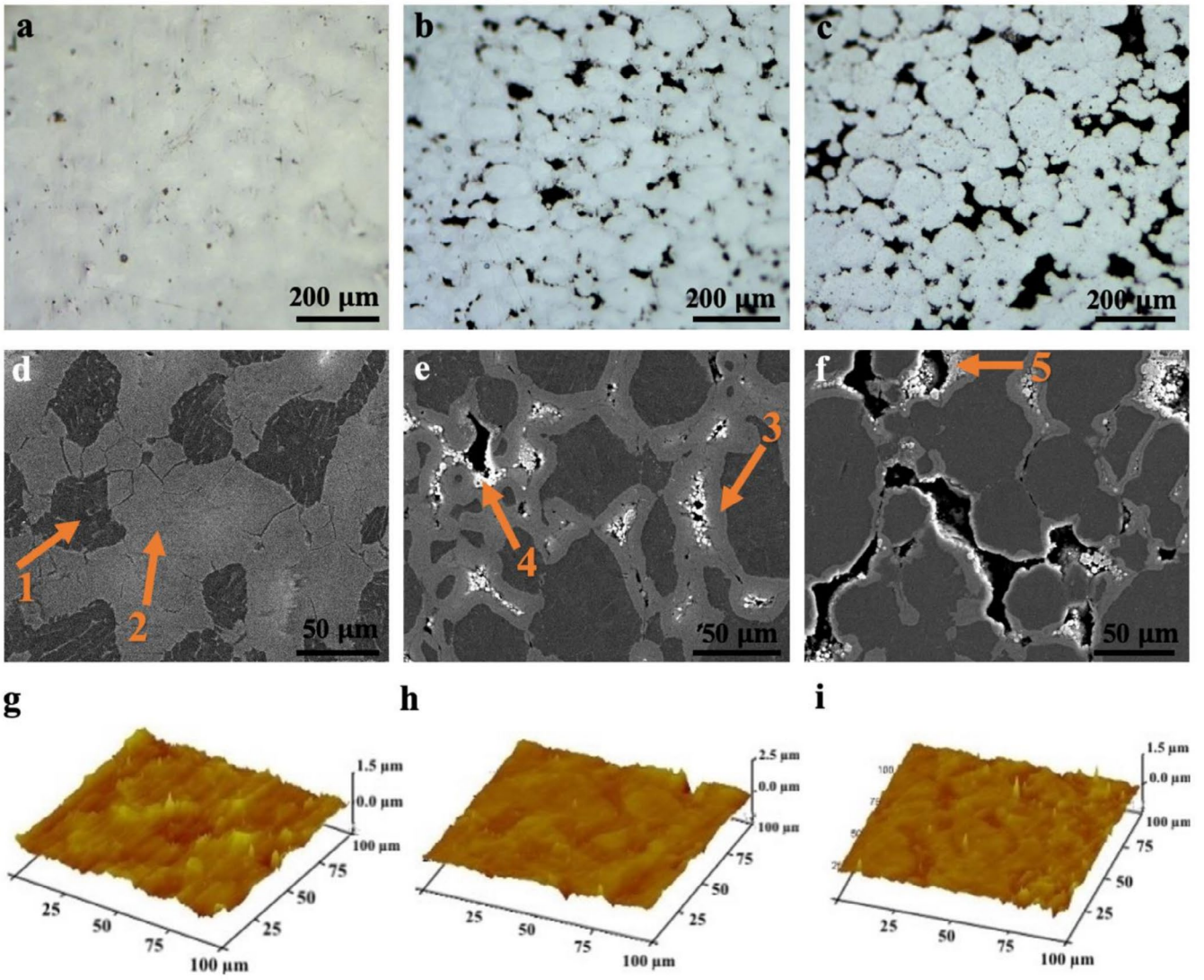


FIGURE 4 | OM, SEM and AFM image of inner layer (a, d, g), OM, SEM and AFM image of middle layer (b, e, h), OM, SEM and AFM image of outer layer (c, f, i).

15524965, 2025, 11, Downloaded from https://onlinelibrary.wiley.com/doi/10.1002/jbm.a.38007 by ibrahim mutlu - Kocaeli Üniversitesi , Wiley Online Library on [03/11/2025]. See the Terms and Conditions (https://onlinelibrary.wiley.com/terms-and-conditions) on Wiley Online Library for rules of use; OA articles are governed by the applicable Creative Commons License

TABLE 5 | AFM 3D simulation roughness values of Ti-5Mo/HA.

Material	R_q, nm	R_a, nm	R_{max}, nm	K, nm	Ref.
Ti-6Al-4V	75.1 ± 15.3	53.8 ± 126	655.08	−0.347	[28]
Inner layer (TiMo)	145.25 ± 23.4	103 ± 19	1662	0.391	This study
Middle layer (TiMo5HA)	154 ± 15.5	109 ± 4.9	2720	−1.59	This study
Outer layer (TiMo10HA)	272 ± 96.9	148 ± 41	3050	−3.91	This study

Abbreviations: R_q = root mean square of roughness, R_a = arithmetic mean of roughness, R_{max} = maximum peak height, K = Skewness.

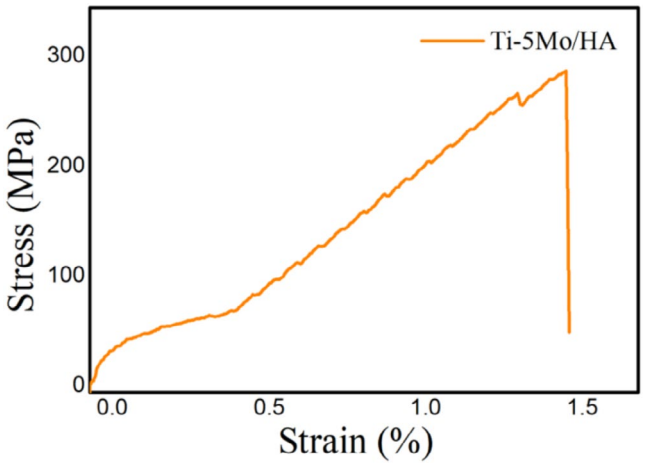


FIGURE 5 | Three-point bending test graph of Ti-5Mo/HA FGM.

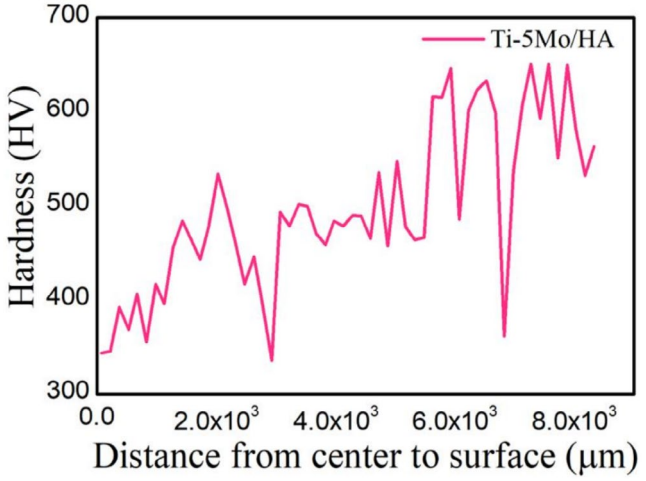


FIGURE 6 | Vickers hardness graph of Ti-5Mo/HA FGM.

hardness, and wear tests, to assess its suitability for bioactive implant interfaces.

The value of the maximum load was obtained at 29.4 kN in the Brazilian splitting tensile test. Using this value in Equation (1), the calculated splitting tensile strength was 187.3 MPa, substantially lower than the tensile strength of conventional Ti-6Al-4V alloys (987 MPa). This reduction is mainly due to the structural inhomogeneity introduced by the HA phase and its low fracture toughness [30]. However, this mechanical trade-off is acceptable in biomedical applications where enhanced bioactivity is prioritized over pure mechanical strength.

To further investigate the mechanical behavior, three-point bending tests were conducted, as shown in Figure 5. The stress–strain response of the Ti-5Mo/HA composite exhibited an initial linear elastic region, followed by a noticeable inflection and a sudden decline post-yielding. This deviation from idealized monotonic behavior is likely attributed to the radially graded structure of the composite. In such graded systems, the inhomogeneous distribution of phases and mechanical properties across the cross-section leads to multi-stage deformation and stress redistribution under bending loads. The core region, dominated by metallic Ti and Mo phases, sustains the primary load initially, whereas the outer HA-rich layer, being more brittle, contributes to the early onset of localized failure mechanisms. The maximum bending strength was recorded as 292 MPa, which is significantly lower than that of the Ti-6Al-4V alloy (1762 MPa) and the Ti-6Al-4V alloy with 5 wt.% Mo (1759 MPa) [15]. This reduction aligns with prior studies indicating that the incorporation of HA severely reduces bending strength due to its low fracture toughness (36.89 MPa) [31]. Despite the lower strength, the bending elastic modulus of Ti-5Mo/HA was calculated as 22.4 GPa, closely matching the range of natural cortical bone (17–30 GPa) [32]. This compliance with bone elasticity is beneficial for reducing stress shielding, thereby enhancing bone remodeling and long-term implant integration.

The hardness distribution of the Ti-5Mo/HA functionally graded composite, measured along a radial line from the center to the outer surface at 150 μm intervals, is presented in Figure 6. The hardness values progressively increased from 336.5 HV in the core to 650.8 HV at the outer layer, reflecting the intended compositional gradient driven by the increasing HA content toward the periphery [33]. The average hardness values of the inner, middle, and outer regions were calculated as 378.2, 471.7, and 578.5 HV, respectively. This gradient is advantageous, providing a strong metallic core for mechanical load-bearing and a hard, HA-enriched outer surface that enhances wear resistance and surface performance.

While a general upward trend is observed, the curve exhibits notable fluctuations, particularly in the middle and transition zones. These variations may be attributed to localized phase heterogeneity, microstructural porosity, or surface roughness effects, commonly encountered in FGM systems incorporating brittle ceramic reinforcements. Additionally, the presence of HA may lead to microcracking or uneven densification, which can introduce scatter in the hardness data. A detailed analysis of standard deviations and transition behaviors is provided in Figure S6, supporting the observed gradient and validating the layer-wise hardness differentiation.

15524965, 2025, 11, Downloaded from https://onlinelibrary.wiley.com/doi/10.1002/jbm.a.38007 by ibrahim mutlu - Kocaeli Üniversitesi , Wiley Online Library on [03/11/2025]. See the Terms and Conditions (https://onlinelibrary.wiley.com/terms-and-conditions) on Wiley Online Library for rules of use; OA articles are governed by the applicable Creative Commons License

The tribological performance of the Ti-5Mo/HA FGM was evaluated under both dry and corrosive conditions to simulate mechanical wear in physiological and non-physiological environments. As shown in Figure 7, the coefficient of friction remained relatively stable over the entire sliding distance of 100 m, with average values of 0.54 (dry) and 0.53 (corrosive). Although these values are higher than those typically reported for Ti-6Al-4V alloys (~0.4), the Ti-5Mo/HA composite exhibited lower wear volumes (1.89 mm^3 in dry and 2.26 mm^3 in corrosive media) corresponding to specific wear rates of 9.5×10^{-4} mm^3/N.m and 11.3×10^{-4} mm^3/N.m, respectively.

This counterintuitive behavior, where a higher friction coefficient coexists with a lower wear rate, can be attributed to the formation of hard, protective surface layers. XRD analysis confirmed the presence of TiO, Ti_6O, and TiPO phases, which are known to act as tribological barriers. Furthermore, the incorporation of HA contributes to surface hardening, limiting material removal during repeated sliding. These results demonstrate that the graded surface composition and oxide film formation synergistically enhance the wear resistance of the composite. Such characteristics are highly desirable in biomedical implants, where consistent friction and low wear are critical for maintaining long-term functionality and minimizing particle-induced inflammation [34].

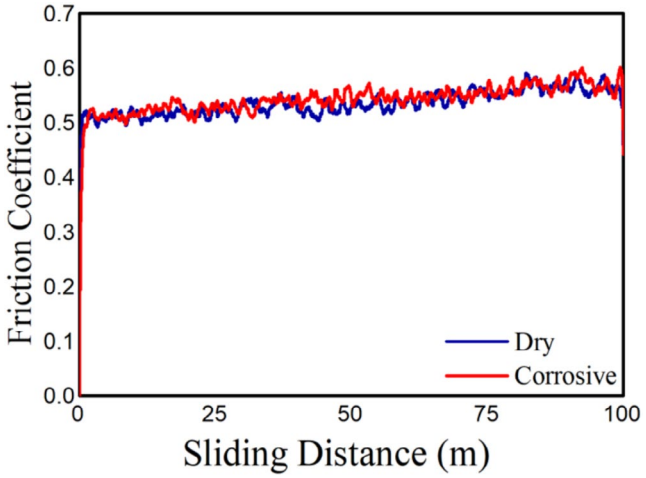


FIGURE 7 | Friction-coefficient graph of Ti-5Mo/HA FGM.

4.1 | Wettability Analysis Results

The wettability behavior of the Ti-5Mo/HA functionally graded composite was characterized by static and dynamic contact angle measurements. As shown in Figure 8a, the static contact angle (θ_E) was measured as 35.35° ± 2°, indicating significantly improved hydrophilicity compared to conventional Ti-based alloys. Dynamic measurements, including ACA, RCA, and CAH, are summarized in Table 6. Notably, the ACA and RCA values of Ti-5Mo/HA were reduced by 15.2% and 29.3%, respectively, relative to those of Ti-6Al-4V [35]. The greater reduction in RCA, known to be more sensitive to surface topography, suggests enhanced surface roughness and chemical reactivity, both favorable for biological performance [36].

CAH, defined as the difference between ACA and RCA, serves as an indicator of liquid–surface interaction dynamics [37]. Higher CAH values typically reflect increased surface adhesion and stronger hydrophilicity. In this study, the Ti-5Mo/HA FGM demonstrated a higher CAH than Ti-6Al-4V [35], likely due to the presence of hydroxyl-rich hydroxyapatite (HA) on the surface. These groups facilitate protein adsorption and osteoblast attachment, supporting enhanced bioactivity and improved osseointegration.

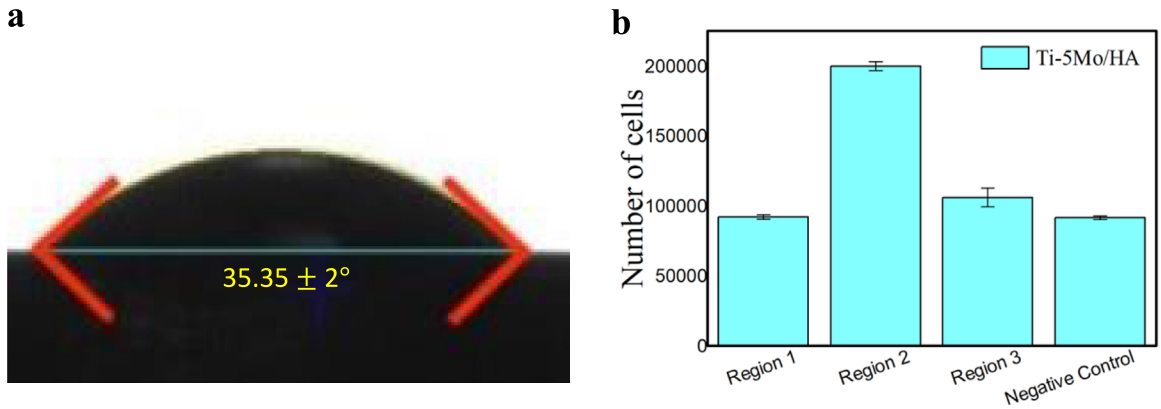


FIGURE 8 | Equilibrium contact angle (a), cell attachment data following 24 h incubation (b). The significance level observed is $*p < 0.05$ in comparison with the control group.

TABLE 6 | Contact angle results of Ti-5Mo/HA FGM.

Material	θ_E (°)	θ_{ACA} (°)	θ_{RCA} (°)	CAH (°)	Ref.
Ti-5Mo/HA	35.35 ± 2.3	42.2 ± 2.8	28.4 ± 1.7	13.8	This study
Ti-6Al-4V	—	49.8 ± 1.1	40.2 ± 0.6	9.6	[38]

15524965, 2025, 11, Downloaded from https://onlinelibrary.wiley.com/doi/10.1002/jbm.a.38007 by ibrahim mutlu - Kocaeli Üniversitesi , Wiley Online Library on [03/11/2025]. See the Terms and Conditions (https://onlinelibrary.wiley.com/terms-and-conditions) on Wiley Online Library for rules of use; OA articles are governed by the applicable Creative Commons License

4.2 | Cytotoxicity Evaluation

To assess the influence of compositional gradation on cellular behavior, the cytotoxicity of the Ti-5Mo/HA FGM was evaluated in vitro using L929 mouse fibroblast cells. As described in the experimental section, Regions 1, 2, and 3 were incubated with the cells, and the resulting cell proliferation, expressed as the number of viable cells, is shown in Figure 8b. Among the test groups, Region 2 exhibited significantly higher cell viability compared to Regions 1 and 3. Since Ti-5Mo/HA has a non-homogeneous structure, regions 1, 2, and 3 have equal size but different compositions in different sections of the sample. So, even though they were cut from the same material, this high cell viability in Region 2 is likely attributed to its relatively higher HA content, which is known to promote favorable biological responses through its bioactive surface chemistry. These findings align with previous studies reporting the positive effect of HA on osteoblast proliferation and protein adsorption [37, 38]. Nevertheless, since topographical analysis or qualitative assessment could not be performed in the scope of this study, examining the effect of the changing HA ratio on cell viability is a possible future study.

Notably, all Ti-5Mo/HA regions demonstrated cell proliferation levels comparable to or greater than the negative control group, confirming the non-cytotoxic nature of the composite. The combination of titanium's mechanical performance and HA's bioactivity suggests that the Ti-5Mo/HA FGM has considerable potential as a next-generation bioimplant material, particularly in applications requiring enhanced early-stage cell adhesion and proliferation.

5 | Discussion

There is a great demand for multifunctional biomaterials that could provide maximum integration with living tissue for orthopedic applications. While Ti-6Al-4V already exists as a suitable material for orthopedic applications, it is plagued by poor mechanical properties and osseointegration issues. Here, we described the development of functionalized material, with improved bioactivity and a reduced mismatch between implant and living tissue, by using a hot-pressing technique. Then, conducting comprehensive analyses (metallurgical, mechanical, and cytotoxicity performance) to understand and predict its performance as an orthopedic material. It is important to mention that the design features a radially graded biomaterial that transitions from the inner layer with high mechanical strength to the outer layer with high bioactivity and low hardness. Also, difficulties during the molding stage of the relevant powder material were a limiting factor for the radially graded processes compared to alternative molding methods.

XRD patterns confirmed the characteristic crystalline structure of the Ti-5Mo/HA, including β-type Ti. It is evident that the phase transition of Ti occurred with the presence of the reflection of the -phase, a cubic lattice structure. Furthermore, the Rietveld refinement clearly indicates the presence of the -phase with 49.4% of the structure shown to be stabilized in the + α″ phase, result which is significantly better than traditional methods that do not allow for this stabilization. The and α″ phases enable us to obtain a structure that has reduced hardness when compared to the α phase. By calculating the phase ratio, we were able to accurately determine the qualities of our novel-produced material, resulting in effective and reliable results. SEM images enable us to observe the structural variations in different layers, the transition between the layers and the position of Mo and HA among the Ti-6Al-4V particles. Based on the EDX mapping analysis, it is apparent that Ti, Al and V are concentrated in the same region while Mo particles are distributed among major grain boundaries (Figures S1–S3). Furthermore, certain regions exhibited varying Ti and Mo amounts which could be due to different times required time for the diffusion and solubility. According to Figures S1–S3, Mo concentration is effective not only in the border region of the construction but also in the Mo and HA particles that can be seen between Ti particles. A high concentration of calcium and phosphorus in the interstitial spaces resembles pores. As observed in both SEM and AFM, the surface morphology of the Ti-5Mo/HA layers with increased HA content was rougher than the inner layer.

The adhesion of implant material to the living tissue has a significant impact on the biomaterial's functionality, and inadequate integration could lead to the implants' instability. Hence, surface topography is an important element in implant integration; the surface topography of the produced Ti-5Mo/HA was also investigated in this study. Surface roughness and complex microstructures improve bone-to-implant contact and promote cell proliferation on the implant material. This study determined that Ti-5Mo/HA had enhanced surface roughness values compared to Ti-6Al-4V. Furthermore, all roughness values gradually increase toward the outer layer, the most active region between the tissue and the implant. While surface roughness is a significant component, it is not sufficient alone to determine the level of cell viability. The negative skewness (K) value of the surface topography is another critical factor in enhancing cell adhesion. The negative K value has been determined as a significant factor in cell viability, and decreasing the K positively affects cell adhesion. As shown in Table 5, Ti-5Mo/HA clearly exhibits decreasing K values toward the outer layer that indicate higher cell proliferation potential [39].

In addition, through rigorous mechanical evaluation, it was confirmed that the Ti-5Mo/HA biomaterial possesses sufficient strength to withstand physiological loads seen in orthopedic applications and has a mechanical similarity to living tissue owed to the graded structure. We also examined the effect of Mo and HA content on the dry and corrosive sliding wear properties of Ti-5Mo/HA. The most important effect of Mo on the Ti-6Al-4V alloy can be seen in its wear resistance [15]. This improvement in wear resistance can be attributed to the formation of a film on the alloy's surface. This superior film develops on the surface of Ti-Mo alloys and exhibits superior wear resistance compared to the passive film formed on pure Ti. HA, with its characteristic structural hardness typical of ceramics, can also contribute to the wear resistance enhancement.

Ti-5Mo/HA surface's ACA and RCA characteristics indicate that the graded structure and the HA content, which were distributed in the middle and outer layers, significantly improved the wetting characteristics. This provides positive results for the osseointegration rates and cellular adaptation. To ensure

15524965, 2025, 11, Downloaded from https://onlinelibrary.wiley.com/doi/10.1002/jbm.a.38007 by ibrahim mutlu - Kocaeli Üniversitesi , Wiley Online Library on [03/11/2025]. See the Terms and Conditions (https://onlinelibrary.wiley.com/terms-and-conditions) on Wiley Online Library for rules of use; OA articles are governed by the applicable Creative Commons License

a successful application, the implant material-host interaction should be evaluated by the modern test systems. Ti-5Mo/HA materials were placed in an L929 mouse fibroblast cell culture for the cytotoxicity evaluation. Cytotoxicity test results confirm the positive cellular response. Thus, providing that Ti-5Mo/HA encouraged much higher cell viability while Ti-6Al-4V had almost half of Ti-5Mo/HA [38].

6 | Conclusion

In this study, a novel radially functionally graded Ti-5Mo/HA composite was successfully fabricated via powder metallurgy and vacuum hot pressing, aiming to optimize both mechanical performance and biological compatibility for load-bearing implant applications. The graded structure enabled a gradual transition from a ductile Ti-Mo metallic core to a HA-enriched bioactive surface, mimicking the natural bone implant interface.

The material demonstrated a bending modulus of 22.4 GPa closely aligned with that of cortical bone while maintaining adequate hardness and wear resistance at the surface. Furthermore, the increased surface roughness and hydrophilicity, coupled with enhanced cell viability, validated the biological potential of the design. The successful stabilization of the β-phase via Mo addition and the selective phase transformation were confirmed by XRD and SEM–EDX analyses.

These findings underline the promise of the Ti-5Mo/HA FGM as a next-generation biomaterial for orthopedic and dental implants. Future studies may focus on long-term in vivo evaluations and fatigue behavior under cyclic loading conditions to further validate its clinical applicability.

Acknowledgments

This work was supported by the Scientific Research Project Unit of Kocaeli University (FDK-2023-3445, FHD-2024-3657) and TUBITAK (The Scientific and Technological Research Council of Türkiye) (2211-C 2023/1, 2214-A 2023/2).

Conflicts of Interest

The authors declare no conflicts of interest.

Data Availability Statement

The data that support the findings of this study are available from the corresponding author upon reasonable request.

References

1. E. Yılmaz, F. Kabataş, A. Gökçe, and F. Fındık, "Production and Characterization of a Bone-Like Porous Ti/Ti-Hydroxyapatite Functionally Graded Material," *Journal of Materials Engineering and Performance* 29, no. 10 (October 2020): 6455–6467, https://doi.org/10.1007/s11665-020-05165-2.

2. E. Yılmaz, A. Gökçe, F. Findik, and H. Ö. Gulsoy, "Assessment of Ti–16Nb–xZr Alloys Produced via PIM for Implant Applications," *Journal of Thermal Analysis and Calorimetry* 134, no. 1 (October 2018): 7–14, https://doi.org/10.1007/s10973-017-6808-0.

3. L.-C. Zhang, L.-Y. Chen, S. Zhou, and Z. Luo, "Powder Bed Fusion Manufacturing of Beta-Type Titanium Alloys for Biomedical Implant Applications: A Review," *Journal of Alloys and Compounds* 936 (March 2023): 168099, https://doi.org/10.1016/j.jallcom.2022.168099.

4. J. M. Wilkinson, A. J. Hamer, A. Rogers, I. Stockley, and R. Eastell, "Bone Mineral Density and Biochemical Markers of Bone Turnover in Aseptic Loosening After Total Hip Arthroplasty," *Journal of Orthopaedic Research* 21, no. 4 (July 2003): 691–696, https://doi.org/10.1016/S0736-0266(02)00237-1.

5. A. Sola, D. Bellucci, and V. Cannillo, "Functionally Graded Materials for Orthopedic Applications—An Update on Design and Manufacturing," *Biotechnology Advances* 34, no. 5 (September 2016): 504–531, https://doi.org/10.1016/j.biotechadv.2015.12.013.

6. A. Dubey, S. Jaiswal, and D. Lahiri, "Promises of Functionally Graded Material in Bone Regeneration: Current Trends, Properties, and Challenges," *ACS Biomaterials Science & Engineering* 8, no. 3 (March 2022): 1001–1027, https://doi.org/10.1021/acsbiomaterials.1c01416.

7. H. Shi, P. Zhou, J. Li, C. Liu, and L. Wang, "Functional Gradient Metallic Biomaterials: Techniques, Current Scenery, and Future Prospects in the Biomedical Field," *Frontiers in Bioengineering and Biotechnology* 8 (January 2021): 616845, https://doi.org/10.3389/fbioe.2020.616845.

8. X. Wang, C. Wan, X. Feng, F. Zhao, and H. Wang, "In Vivo and in Vitro Analyses of Titanium-Hydroxyapatite Functionally Graded Material for Dental Implants," *BioMed Research International* 2021 (2021): 1–14, https://doi.org/10.1155/2021/8859945.

9. H. Jaber and T. Kovacs, "Selective Laser Melting of Ti Alloys and Hydroxyapatite for Tissue Engineering: Progress and Challenges," *Materials Research Express* 6, no. 8 (May 2019): 82003, https://doi.org/10.1088/2053-1591/ab1dee.

10. B. H. B. Kuffner, P. Capellato, L. M. S. Ribeiro, D. Sachs, and G. Silva, "Production and Characterization of a 316L Stainless Steel/β-TCP Biocomposite Using the Functionally Graded Materials (FGMs) Technique for Dental and Orthopedic Applications," *Meta* 11, no. 12 (2021): 1923, https://doi.org/10.3390/met11121923.

11. H. S. Hedia and N. Fouda, "A New Design of Hip Prosthesis Coating Using Functionally Graded Material," *Materials Testing* 55, no. 1 (2013): 23–31, https://doi.org/10.3139/120.110400.

12. C. Sun, L. Wang, J. Kang, D. Li, and Z. Jin, "Biomechanical Optimization of Elastic Modulus Distribution in Porous Femoral Stem for Artificial Hip Joints," *Journal of Bionic Engineering* 15, no. 4 (July 2018): 693–702, https://doi.org/10.1007/s42235-018-0057-1.

13. T. A. Enab, N. Fouda, and I. Eldesouky, "Comparison of Functionally Graded Hip Stem Implants With Various Second-Generation Titanium Alloys," *Journal of Applied and Computational Mechanics* 7, no. 3 (April 2020): 1315–1323.

14. S. Asiri, "Design and Analysis of Cementless Hip-Joint System Using Functionally Graded Material," *Archive of Mechanical Engineering* 69, no. 1 (2021): 129–146, https://doi.org/10.24425/ame.2021.139804.

15. R. Yamanoglu, A. Bahador, and K. Kondoh, "Effect of Mo Addition on the Mechanical and Wear Behavior of Plasma Rotating Electrode Process Atomized Ti6Al4V Alloy," *Journal of Materials Engineering and Performance* 30, no. 5 (May 2021): 3203–3212, https://doi.org/10.1007/s11665-021-05631-5.

16. E. Delvat, D. M. Gordin, T. Gloriant, J. L. Duval, and M. D. Nagel, "Microstructure, Mechanical Properties and Cytocompatibility of Stable Beta Ti–Mo–ta Sintered Alloys," *Journal of the Mechanical Behavior of Biomedical Materials* 1, no. 4 (October 2008): 345–351, https://doi.org/10.1016/j.jmbbm.2008.01.006.

17. F. Xie, X. He, X. Lu, S. Cao, and X. Qu, "Preparation and Properties of Porous Ti–10Mo Alloy by Selective Laser Sintering," *Materials Science and Engineering: C* 33, no. 3 (April 2013): 1085–1090, https://doi.org/10.1016/j.msec.2012.11.037.

15524965, 2025, 11, Downloaded from https://onlinelibrary.wiley.com/doi/10.1002/jbm.a.38007 by ibrahim mutlu - Kocaeli Üniversitesi , Wiley Online Library on [03/11/2025]. See the Terms and Conditions (https://onlinelibrary.wiley.com/terms-and-conditions) on Wiley Online Library for rules of use; OA articles are governed by the applicable Creative Commons License

18. ASTM C496/C496M-17, *Annual Book of ASTM Standarts*, vol. 4, 2nd ed. (ASTM International, 2017), 290–294.

19. E. M. Borisovskaya, V. A. Nazarenko, Y. N. Podrezov, O. S. Koryak, Y. I. Evich, and A. V. Vdovichenko, "Mechanical Properties of Powder Titanium at Different Production Stages. II. Mechanical Behavior of Porous Titanium Compacts," *Powder Metallurgy and Metal Ceramics* 47, no. 9–10 (September 2008): 538–545, https://doi.org/10.1007/s11106-008-9056-9.

20. F. Jiang, R. M. Kulin, and K. S. Vecchio, "Use of Brazilian Disk Test to Determine Properties of Metallic-Intermetallic Laminate Composites," *JOM* 62, no. 1 (2010): 35–40, https://doi.org/10.1007/s11837-010-0008-8.

21. S. K. Ray, A. Banerjee, B. K. Bhangi, D. Pyne, and B. Dutta, "Tribological Analysis General Test Standards," in *Tribology of Polymers, Polymer Composites, and Polymer Nanocomposites* (Elsevier, 2023), 17–50, https://doi.org/10.1016/B978-0-323-90748-4.00001-7.

22. W. Wang, J. Li, J.-t. Gu, et al., "Optimization of Lactoferrin-Derived Amyloid Coating for Enhancing Soft Tissue Seal and Antibacterial Activity of Titanium Implants," *Advanced Healthcare Materials* 12, no. 11 (2023): 2203086, https://doi.org/10.1002/adhm.202203086.

23. Y. Feng, D. Wu, J. Knaus, et al., "A Bioinspired Gelatin–Amorphous Calcium Phosphate Coating on Titanium Implant for Bone Regeneration," *Advanced Healthcare Materials* 12, no. 20 (2023): 2203411, https://doi.org/10.1002/adhm.202203411.

24. R. A. Gittens, L. Scheideler, F. Rupp, et al., "A Review on the Wettability of Dental Implant Surfaces II: Biological and Clinical Aspects," *Acta Biomaterialia* 10, no. 7 (July 2014): 2907–2918, https://doi.org/10.1016/j.actbio.2014.03.032.

25. Y. Hirakawa, R. Jimbo, Y. Shibata, I. Watanabe, A. Wennerberg, and T. Sawase, "Accelerated Bone Formation on Photo-Induced Hydrophilic Titanium Implants: an Experimental Study in the Dog Mandible," *Clinical Oral Implants Research* 24, no. A100 (August 2013): 139–144, https://doi.org/10.1111/j.1600-0501.2011.02401.x.

26. G. Lütjering, J. C. Williams, G. Lütjering, and J. C. Williams, *Titanium Matrix Composites* (Springer, 2003).

27. Y. Qiao, D. Xu, S. Wang, et al., "Corrosion and Tensile Behaviors of Ti-4Al-2V-1Mo-1Fe and Ti-6Al-4V Titanium Alloys," *Metals (Basel)* 9, no. 11 (November 2019): 1213, https://doi.org/10.3390/met9111213.

28. J. I. Rosales-Leal, M. A. Rodríguez-Valverde, G. Mazzaglia, et al., "Effect of Roughness, Wettability and Morphology of Engineered Titanium Surfaces on Osteoblast-Like Cell Adhesion," *Colloids and Surfaces A: Physicochemical and Engineering Aspects* 365, no. 1–3 (August 2010): 222–229, https://doi.org/10.1016/j.colsurfa.2009.12.017.

29. A. Khorasani, I. Gibson, U. S. Awan, and A. Ghaderi, "The Effect of SLM Process Parameters on Density, Hardness, Tensile Strength and Surface Quality of Ti-6Al-4V," *Additive Manufacturing* 25 (January 2019): 176–186, https://doi.org/10.1016/j.addma.2018.09.002.

30. Z. M. Xiu, Y. Liu, J. G. Li, et al., "Fabrication and Properties of Hydroxyapatite-Ti Network Composites," *Advanced Materials Research* 41–42 (2008): 41–48, https://doi.org/10.4028/www.scientific.net/AMR.41-42.41.

31. J. Zhao, Z. Wang, L. Tian, et al., "Study on Mechanical Properties of Ti-6Al-4 V Titanium Alloy With Different Microstructures Under Combined Tension-Bending Load," *Journal of Alloys and Compounds* 936 (March 2023): 168201, https://doi.org/10.1016/j.jallcom.2022.168201.

32. F. X. Xie, X. B. He, S. L. Cao, X. Lu, and X. H. Qu, "Structural Characterization and Electrochemical Behavior of a Laser-Sintered Porous Ti–10Mo Alloy," *Corrosion Science* 67 (February 2013): 217–224, https://doi.org/10.1016/j.corsci.2012.10.036.

33. Y. Chen, L. Xu, Z. Liu, F. Kong, and Z. Chen, "Microstructures and Properties of Titanium Alloys Ti-Mo for Dental Use," *Transactions of Nonferrous Metals Society of China* 16 (2006): s824–s828, https://doi.org/10.1016/S1003-6326(06)60308-7.

34. Y. Yan, E. Chibowski, and A. Szcześ, "Surface Properties of Ti-6Al-4V Alloy Part I: Surface Roughness and Apparent Surface Free Energy," *Materials Science and Engineering: C* 70 (January 2017): 207–215, https://doi.org/10.1016/j.msec.2016.08.080.

35. T. Huhtamäki, X. Tian, J. T. Korhonen, and R. H. A. Ras, "Surface-Wetting Characterization Using Contact-Angle Measurements," *Nature Protocols* 13, no. 7 (July 2018): 1521–1538, https://doi.org/10.1038/s41596-018-0003-z.

36. O. Carrier and D. Bonn, "Contact Angles and the Surface Free Energy of Solids," in *Droplet Wetting and Evaporation* (Elsevier, 2015), 15–23, https://doi.org/10.1016/B978-0-12-800722-8.00002-3.

37. X. Zhou, D. Xu, S. Geng, et al., "Mechanical Properties, Corrosion Behavior and Cytotoxicity of Ti-6Al-4V Alloy Fabricated by Laser Metal Deposition," *Materials Characterization* 179 (September 2021): 111302, https://doi.org/10.1016/j.matchar.2021.111302.

38. E. Velasco-Ortega, A. Jos, A. M. Cameán, J. Pato-Mourelo, and J. J. Segura-Egea, "In Vitro Evaluation of Cytotoxicity and Genotoxicity of a Commercial Titanium Alloy for Dental Implantology," *Mutation Research, Genetic Toxicology and Environmental Mutagenesis* 702, no. 1 (September 2010): 17–23, https://doi.org/10.1016/j.mrgentox.2010.06.013.

39. J. Havlikova, J. Strasky, M. Vandrovcova, et al., "Innovative Surface Modification of Ti–6al–4v Alloy with a Positive Effect on Osteoblast Proliferation and Fatigue Performance," *Materials Science and Engineering: C* 39 (2014): 371–379, https://doi.org/10.1016/j.msec.2014.03.024.

Supporting Information

Additional supporting information can be found online in the Supporting Information section. **Data S1:** jbma38007-sup-0001-Supinfo.pdf.

15524965, 2025, 11, Downloaded from https://onlinelibrary.wiley.com/doi/10.1002/jbm.a.38007 by ibrahim mutlu - Kocaeli Üniversitesi , Wiley Online Library on [03/11/2025]. See the Terms and Conditions (https://onlinelibrary.wiley.com/terms-and-conditions) on Wiley Online Library for rules of use; OA articles are governed by the applicable Creative Commons License